lajss.org
Latin American Journal of Solids and Structures
www.lajss.org

Analysis of vulnerability curves and surfaces of storage tanks considering vector seismic motion parameters

Yi Yang[a,b], Jianchun Xiao[a,b*] ORCID ID, Cong Liu[a,b],Jun Wang[c]

[a] Space Structures Research Center, Guizhou University, Guiyang 550025, China. Email: 2264660458@qq.com, jcxiao@gzu.edu.cn, 1346710574@qq.com, 207175816@qq.com

[b] Guizhou Province Key Laboratory of Green Building and Intelligent Construction, Guiyang 550025, China

[c] Sinohydro Bureau 9 Co., Ltd., Guiyang 550081, China

* Corresponding author

Abstract

Storage tanks are key equipment for storing and managing liquids in industrial production. Their seismic performance evaluation is often carried out through the failure probability of vulnerability analysis. However, the vulnerability curve obtained from a single seismic component will increase the uncertainty of the evaluation, and the seismic analysis of large-capacity storage tanks has problems such as complex models and large calculations. Therefore, this paper adopts Edurance Tme Aalysis (ETA) to effectively evaluate the seismic performance of storage tanks, and verifies the effectiveness of this method by performing incremental dynamic analysis on 22 selected near-field seismic waves. Using the idea of ETA, the endurance time and seismic motion parameters are converted to derive the dynamic response of the second seismic motion parameter. Subsequently, scalar fragility curve analysis is performed for the two seismic motion parameters respectively, and then vector fragility surface analysis is performed in combination with these two parameters. The research results show that ETA can approximately determine the ultimate seismic performance of storage tanks through a single dynamic analysis, highlighting its effectiveness and efficiency in the dynamic response evaluation of storage tank structures. The surface morphology under different damage states shows a gradient change, with the surface of slight damage being the steepest and the surface of severe damage being the slowest. Compared with the scalar fragility curve, the vector fragility surface can enhance the reliability of probability and significantly reduce the uncertainty of the danger curve in structural response analysis. The fragility surface can not only be converted into a conventional fragility curve, but also complete the multi-dimensional characteristics of the seismic motion. The research results provide a more comprehensive and accurate quantitative analysis method for the evaluation of the seismic performance of liquid storage tanks.

Keywords:

Vulnerability curve, Vulnerability surface, Storage tank, Endurance time analysis, Incremental dynamic analysis

1. Introduction

Liquid storage tanks have a crucial role in contemporary architectural settings. Their extensive distribution and diverse applications prove their critical role in the storage and distribution of essential resources(Alessandri et al, 2018; De Angelis et al, 2010; Merino Vela et al, 2019).In recent decades, the instability of storage tanks due to several earthquakes has caused significant economic losses, hampered infrastructure operations, and resulted in major secondary disasters. The 1999 Izmit earthquake in Turkey, the 2003 Tokachi-Oki earthquake in Japan, and the 2012 Emilia earthquake in Italy all demonstrated the susceptibility of liquid storage tanks during seismic events and the potentially disastrous outcomes they may cause(Brunesi et al, 2015; Matsui, 2009; Tavakoli Joorabi and Razzaghi, 2019).The implementation and advancement of performance-based seismic design principles in energy storage need comprehensive study on the seismic vulnerability of storage tanks, an essential consideration(Chiang and Wong, 2014; Merino Vela et al, 2018).

Seismic vulnerability analysis quantitatively describes the seismic performance of structures through probabilistic methods. Its basic concept is to evaluate the conditional probability of a structure reaching or exceeding different limit states of damage under different levels of ground motion intensity measure (IM)(Cornell et al, 2002).When conducting vulnerability analysis, the first step is to select an appropriate IM, and the choice of IM is closely related to the Probabilistic Seismic Demand Model (PSDM).At the same time, IM can enhance the accuracy of generating fragility curves, thereby reducing the uncertainty in evaluating structural responses(He et al, 2022).Therefore, the selection of the seismic intensity parameter IM plays an important role in the seismic vulnerability analysis of storage tanks. In vulnerability analysis, commonly used IMs are mainly divided into two categories: one is scalar IM, which involves analysis using a single IM; the other is vector IMs, which involve analysis using multiple IMs (Argyroudis and Pitilakis, 2012).Currently, the application of scalar IM is relatively widespread, while the use of vector IMs is relatively rare.Bektaş and Aktaş(2023), Erkmen(2024), Miladi et al(2022), Kildashti et al(2018), Vasquez Munoz and Dolšek(2024), and Hajimehrabi et al(2019) have all conducted seismic vulnerability analyses on different storage tanks using scalar IMs (such as PGA and Sa). The resulting seismic vulnerability curves can be used to assess the seismic risk analysis of the corresponding storage tanks. However, the experiments all employed scalar IM expansion. Conversely, the intricate nature of seismic motion renders a singular scalar intensity measure inadequate for encapsulating additional seismic intensity data, leading to a substantial divergence between the anticipated seismic performance of the storage tank and its actual performance (Akköse et al, 2008).In contrast to scalar intensity measures, vector intensity measures more precisely represent the uncertainty of seismic motion, resulting in a stronger correlation between their anticipated seismic performance of storage tanks and actual performance. Presently, most of the domestic and international research employs vulnerability curves derived from a singular intensity measure (IM) to assess the seismic performance of buildings. However, previous studies reveal that the scalar value of IM may not represent the essential seismic properties. Relying solely on a singular intensity metric in vulnerability curves fails to sufficiently evaluate the influence of seismic features on the likelihood of structural collapse (Huang et al, 2021; Wang et al, 2018).

At present, most researchers use computationally intensive analysis methods to evaluate the seismic performance of storage tanks, such as the Icremental Dnamic Aalysis (IDA) method. The IDA technique requires multiple amplitude scaling calculations for different earthquake motions, which requires huge computing resources. Estekanchi (2004) innovatively proposed the ETA. The advantage of this method is that it can describe earthquake sequences of different intensities through a single acceleration time history curve, thereby effectively capturing the structural response at different intensities. At present, the ETA method is mainly used in the seismic response research and seismic performance evaluation of steel frame structures and concrete gravity dams Cui et al., 2023; Zhang et al., 2022; Chen et al., 2024), and has achieved positive results in the fields of underground structures and bridge construction (Wang et al., 2024; Huang et al., 2024). However, there are still few studies on the use of the ETA method to evaluate the seismic performance of

liquid storage tanks. If the ETA method can be effectively applied to the seismic analysis of liquid storage tanks, it will significantly improve the traditional seismic performance analysis methods and vulnerability analysis, and provide a more efficient and comprehensive analysis method for the evaluation of the seismic performance of liquid storage tanks.

Based on this, this work examines a 2000 m³ storage tank and suggests an analytical approach for assessing the tank's susceptibility by integrating ETA, which accurately represents the real damage sustained by the tank during seismic events. Initially, 22 seismic waves were chosen, and 3 seismic response time history curves were produced. A finite element model of the storage tank was developed; IDA and ETA were performed independently to gather the seismic response data of the storage tank. Subsequently, utilizing the notion of seismic time history, parameter conversion was executed to derive the seismic response of the second IM, followed by distinct seismic vulnerability studies based on scalar and vector seismic intensity parameters.

2. Vulnerability analysis process for liquid storage tanks

2.1 Overall framework

This study establishes a seismic vulnerability assessment framework for liquid storage tanks by combining ETA and IDA. The proposed framework is shown in Figure 1, and the specific steps are as follows:

(1) Select 22 seismic records as inputs for IDA.

(2) Generate 3 endurance time acceleration curves as inputs for ETA.

(3) Establish a finite element model of the liquid storage tank, conduct IDA and ETA, and extract the seismic response data of the liquid storage tank.

(4) Compare the results of IDA with those of ETA and convert the seismic time to obtain the seismic response of the second parameter.

(5) Use scalar and vector IMs, respectively, to construct the probabilistic seismic demand model of the liquid storage tank for seismic vulnerability analysis.

(6) Use scalar and vector IMs, respectively, to plot the seismic vulnerability curves and surfaces, and compare the content of the surfaces with the curves.

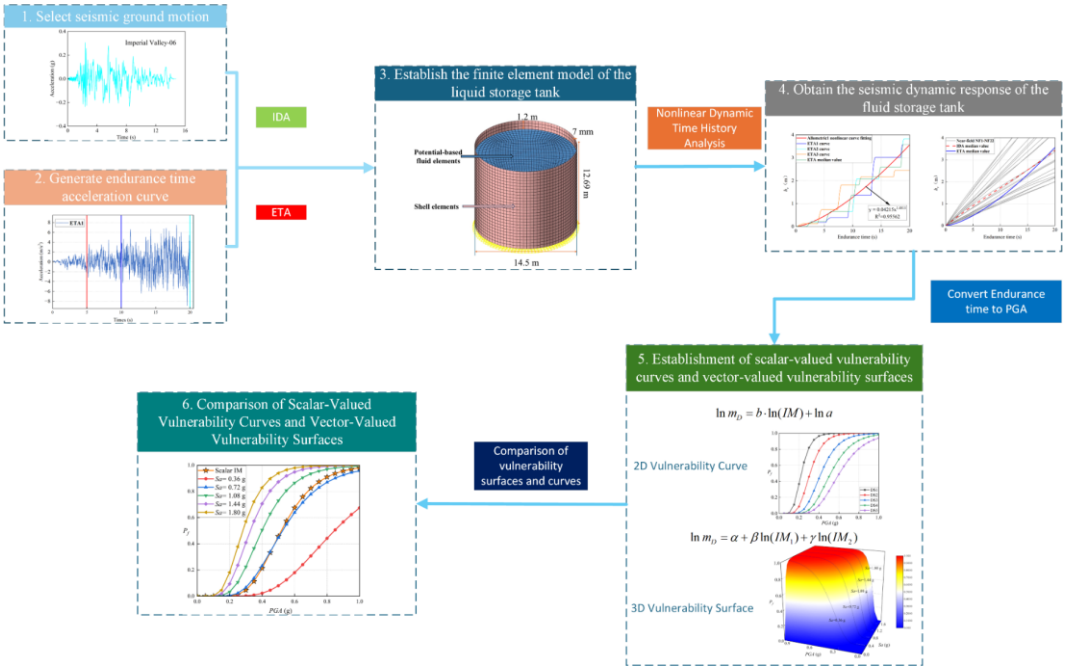

Figure 1 *Framework process for introducing the vulnerability of ETA storage tanks*

2.2 Definition of scalar and vector vulnerability functions

PSDM is a widely utilized and dependable technique for acquiring vulnerability. This approach assesses the seismic performance of structures in a Damage State (DS) for defined levels of ground motion Intensity Measure (IM) and delineates the correlation between Egineering Dmand Prameters (EDP) and IM across various structural types(Baker, 2007). Furthermore, vulnerability curves can offer a definitive and empirical quantitative foundation for the selection of earthquake risk reduction techniques(Chen et al, 2014). To describe the scalar IM of the fragility curve, the log-normal cumulative distribution function is commonly used, as this function can effectively explain the shape of the curve mathematically.

The vulnerability function can be expressed using Eq. 1:

$$P_f(IM = x) = P(EDP > C \mid IM = x) \tag{1}$$

Among them, P_f is the vulnerability function of the structure; *EDP* is the engineering demand parameter, IM is the intensity measure of the seismic motion; *C* is the seismic capacity index of the structure.

The median value of seismic demand (m_D) is typically regarded as adhering to a power-law relationship with seismic intensity(Yu et al, 2021)：

$$m_D = a(IM)^b \tag{2}$$

When employing scalar IM, there exists:

$$\ln m_D = b \cdot \ln(IM) + \ln a \tag{3}$$

ln a and b are the parameters of the logarithmic linear regression.

It is widely accepted that m_D and m_C adhere to a log-normal distribution, as indicated by the formula. Integrating this with the concept of the tank's limit state, the resultant structural seismic vulnerability modeling is delineated as follows, as seen in Eq. 4. Substituting Eq. 3 into Eq. 1 yields the functional formulation of the vulnerability curve.

$$\ln m_D \sim N(u_d, \beta_d^2) \qquad \ln m_C \sim N(u_c, \beta_c^2) \tag{4}$$

$$P_f[D \geq C] = \Phi\left(\frac{\ln a + b\ln(IM) - \ln(m_C)}{\sqrt{\beta_c^2 + \beta_d^2}}\right) \tag{5}$$

In Eq. 5, Φ denotes the standard normal distribution function, m_D signifies the median value of the *EDP*, m_C indicates the median value of the seismic capacity of the liquid storage structure, u_d represents the logarithmic mean of the engineering demand parameter, β_d is the logarithmic standard deviation of the engineering demand parameter, u_c is the logarithmic mean of the seismic capacity parameter, and β_c is the logarithmic standard deviation of the seismic capacity parameter. The values of β_d and β_c in $\sqrt{\beta_d^2+\beta_c^2}$can be acquired statistically or sourced from existing literature. When the fragility curve uses the acceleration spectrum value associated with the structure's basic period as the independent variable, $\sqrt{\beta_d^2+\beta_c^2}$ is designated as 0.4(*Melchers R E. 1999*.). Consequently, this work adopts $\sqrt{\beta_d^2+\beta_c^2}$ as 0.4.

In the context of vector Intensity Measures (IMs), specifically when using two scalar seismic intensity parameters IM1 and IM2 to create vector IMs, m_D may be articulated using the Eq. 6:

$$\ln m_D = \alpha + \beta \ln(IM_1) + \gamma \ln(IM_2) \tag{6}$$

Among them, α, β, and γ are the bilinear logarithmic regression parameters.

Then, the vulnerability surface of the vector-valued IMs can be represented by the following formula:

$$P_f[D \geq C] = \Phi\left(\frac{\alpha + \beta \ln(IM_1) + \gamma \ln(IM_2) - \ln(m_C)}{\sqrt{\beta_c^2 + \beta_d^2}}\right) \quad (7)$$

2.3 Failure modes and damage states of the liquid storage tank

Selecting appropriate response indicators is crucial for evaluating the tank's response during an earthquake and its subsequent vulnerability analysis. Among these indicators, the wave height (h_v), circumferential tensile stress of tank wall (σ_c) and vertical compressive stress at the bottom of tank wall (σ_v) significantly impact the normal operational capacity of the liquid storage structure after an earthquake(Sun et al, 2009). Intense ground vibrations might induce significant agitation of the liquid within the tank, resulting in overflow and potentially jeopardizing the surrounding environment. Furthermore, the tank wall may fracture owing to severe circumferential tensile stress; another prevalent type of damage is wall instability, particularly in elevated tanks. The aforementioned failure types significantly jeopardize tank safety and are intricately linked to seismic design criteria and the choice of tank materials. Table 1 enumerates the attributes of several failure types together with their associated seismic failure criteria.

Table 1 Failure modes and seismic damage guidelines for storage tanks(Sun et al, 2009)

Failure mode	Seismic damage preparedness	Limit equation of state
Liquid storage overflow	h_v is greater than the cut-off value	h_v-h=0
Cyclic tensile damage of tank wall	σ_c is greater than the allowable wall stress	σ_c-σ=0
Tank wall instability	σ_c is greater than the permissible critical stress for tank wall stabilization	σ_v-σ_{cr}=0

Note: where h is the distance from the top surface of the storage liquid in the tank to the top of the tank wall, which is taken as 1.2 m in this paper; σ is the permissible stress of the tank wall in this paper is taken as 235 MPa; σ_{cr} is the permitted critical stress for vertical stability of the tank wall.

The determination of the DS is crucial in shaping the vulnerability curve during vulnerability analysis. The damage condition of a structure can be assessed by damage indicators or seismic response parameters, which objectively characterize the structure's performance level(Sun et al, 2009). This work delineates five limit states—intact, little damage, moderate damage, severe damage, and full damage—along with their respective limit state values to quantitatively assess the vulnerability of various failure scenarios. Table 2 enumerates the detailed descriptions of each damage state together with the associated quantification criteria for the damage indicators in each condition.

Table 2 Subjective assessment of the solidity of storage tanks and signs of damage(Sun et al, 2009)

Structural status	Description of the damage	Damage indicators		
		h_v	σ_c	σ_v
Basically intact (DS1)	The tank wall has no obvious deformation, the connection parts are in good contact and the connection is reliable.	h_v<0.3h	σ_c<σ_s/1.5	σ_v<σ_{cr}/1.5
Slight damage (DS2)	The tank wall has obvious deformation and slight cracks, but it does not affect normal use.	h_v<0.5h	σ_c<0.8σ_s	σ_v<σ_{cr}/1.2
Medium damage (DS3)	The tank wall is greatly deformed, affecting normal operation.	h_v<0.8h	σ_c<σ_s	σ_v<σ_{cr}
Serious damage (DS4)	The tank wall is seriously deformed, the bottom is unstable or seriously bulging, and it needs to be repaired before use.	h_v<1.1h	σ_c<(σ_s+σ_b)/2	σ_v<σ_{cr}/1.5
Total damage (DS5)	The tank wall is cracked, the tank body is overturned, and the system is completely damaged	h_v<1.4h	σ_c<σ_b	σ_v<1.2σ_{cr}

3 Selected ground motion records and the generation of the endurance time acceleration curves (ETACs)

3.1 Selection of ground motion records

Twenty-two sets of near-field ground movements were extracted from the PEER database for the Incremental Dynamic Analysis investigation. Figure 2 illustrates the acceleration response spectrum of the chosen ground movements with a comparison with the respective average and code response spectrum. The average value of the near-field ground motion response spectrum aligns well with the code response spectrum. Figure 3 illustrates several ground motion acceleration curves.

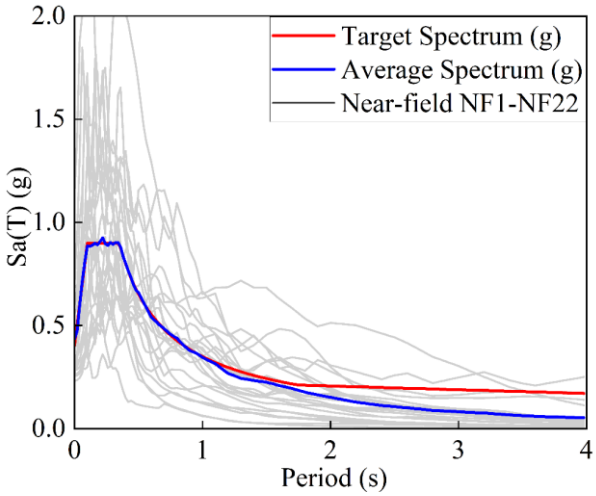

Figure 2 *22 Comparison of Near-Field Motion Response Spectrum and Its Average with Target Response Spectrum*

Table 3 22 near-field motions records

ID	Earthquake Name	Year	Station Name	Magnitude
NF1	Managua_ Nicaragua-01	1972	Managua_ ESSO	6.24
NF2	Gazli_ USSR	1976	Karakyr	6.8
NF3	Imperial Valley-06	1979	Aeropuerto Mexicali	6.53
NF4	Imperial Valley-06	1979	Chihuahua	6.53
NF5	Mammoth Lakes-02	1980	Mammoth Lakes H. S.	5.69
NF6	Corinth_ Greece	1981	Corinth	6.6
NF7	Coalinga-01	1983	Pleasant Valley P.P. - bldg	6.36
NF8	Coalinga-02	1983	Anticline Ridge Free-Field	5.09
NF9	N. Palm Springs	1986	North Palm Springs	6.06
NF10	N. Palm Springs	1986	Whitewater Trout Farm	6.06
NF11	Baja California	1987	Cerro Prieto	5.5
NF12	Northridge-01	1994	Arleta - Nordhoff Fire Sta	6.69
NF13	Northridge-01	1994	Sun Valley - Roscoe Blvd	6.69
NF14	Northridge-01	1994	Sylmar - Olive View Med FF	6.69
NF15	Sierra Madre	1991	Pasadena - USGS/NSMP Office	5.61
NF16	Parkfield-02_ CA	2004	PARKFIELD - MIDDLE MOUNTAIN"	6
NF17	Parkfield-02_ CA	2004	Parkfield - Cholame 3E	6
NF18	Parkfield-02_ CA	2004	Parkfield - Cholame 4AW	6
NF19	Parkfield-02_ CA	2004	Parkfield - Gold Hill 4W	6
NF20	Parkfield-02_ CA	2004	Parkfield - Vineyard Cany 1E	6
NF21	El Mayor-Cucapah_ Mexico	2010	CERRO PRIETO GEOTHERMAL	7.2
NF22	Christchurch_ New Zealand	2011	Hulverstone Drive Pumping Station	6.2

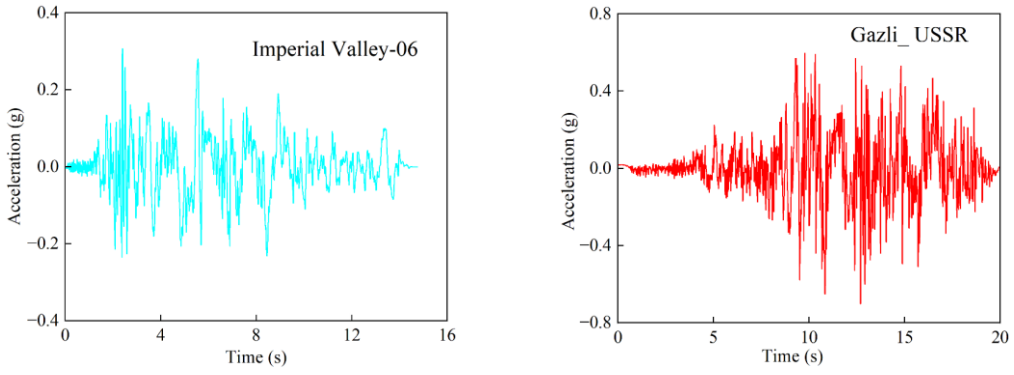

(a) "Imperial Valley-06" (b) "Gazli_ USSR"

Figure 3 *Selected partial seismic acceleration curve records*

3.2 Generation of the ETACs

The essence of the ETA approach entails utilizing a predetermined array of intensity indications that progressively escalate over time, serving as a seismic time history input for the building(Estekanchi et al, 2007). In the ETA approach, by entering an acceleration time history with intensifying magnitude over time, the structural reaction can progressively shift from the linear domain to the nonlinear domain until damage or instability manifests. The synthesis process of this

time history necessitates that the predefined values of the response spectrum and the displacement spectrum exhibit a linear increase over time, which may be expressed by Eq.8 and Eq.9.

$$S_{aT}\left(T,t\right)=\frac{t}{t_{\mathbf{Target}}}S_{aC}\left(T\right) \tag{8}$$

$$S_{\mathbf{uT}}(T,t)=\frac{t}{t_{\mathbf{Target}}}S_{\mathbf{aC}}(T)\times\frac{T^2}{4\pi^2} \tag{9}$$

In Eq.8 and Eq.9, *T* represents the natural period of the structure, while S_{aT}(T,t) and S_{uT}(T,t) refer to the target acceleration response spectrum and target displacement response spectrum within the time period from 0 to *t*.

Meeting the criteria of the endurance time acceleration curve with consistent precision is challenging; so, this issue is reformulated as an unconstrained variable optimization problem, specifically(Nozari and Estekanchi, 2011; Valamanesh et al, 2010):

$$\mathrm{Min}\,F\left(\ddot{u}_g\right)=\int_0^{T\max}\times\int_0^{t\max}\times\begin{Bmatrix}\left[S_{\mathbf{a}}\left(T,t\right)-S_{\mathbf{aT}}\left(T,t\right)\right]^2\\+\alpha\left[S_{\mathbf{u}}\left(T,t\right)-S_{\mathbf{uT}}(T,t)\right]^2\end{Bmatrix}dtdT \tag{10}$$

In Eq.10, $\ddot{u}_g$ represents the target synthetic seismic acceleration time history, and α is used to denote the weight coefficient of the displacement spectrum. S_a(T,t) and S_a(T,t) are the acceleration response spectrum and displacement response spectrum of $\ddot{u}_g$ at any time t with a period of T, respectively. This study employs only the acceleration response spectrum as the target for optimization, setting the weight coefficient *α* to 0.

This study used the design acceleration response spectrum delineated in the "Code for Seismic Design of Buildings" as the reference response spectrum. The parameter values in this research are as follows: α_{max}= 0.90, *Tg* = 0.35, *ζ* = 0.05. The paper generates ETACs with a target time (t_{Target}) of 10 seconds and a duration of 20 seconds, taking into account the influence of site classification on seismic motion and the effect of the site characteristic period (*Tg*) on the response spectrum of China's seismic design code.

Utilize the nonlinear least square's function lsqnonlin inside the MATLAB R2022b Optimization Toolbox to execute unconstrained optimization on Eq.10. Owing to the substantial computational burden of aligning the response spectrum at each time point with the standard target response spectrum during optimization, numerous iterations are performed independently within the time intervals of 0 to 5 seconds, 0 to 10 seconds, and 0 to 20 seconds. The desired damping ratio is established at 5%, with the site characteristic period *Tg* designated as 0.35 seconds. Three ETACs, each having a period of 20 seconds and comprising just the ascending section, were synthesized according to these criteria, as seen in Figure 4.

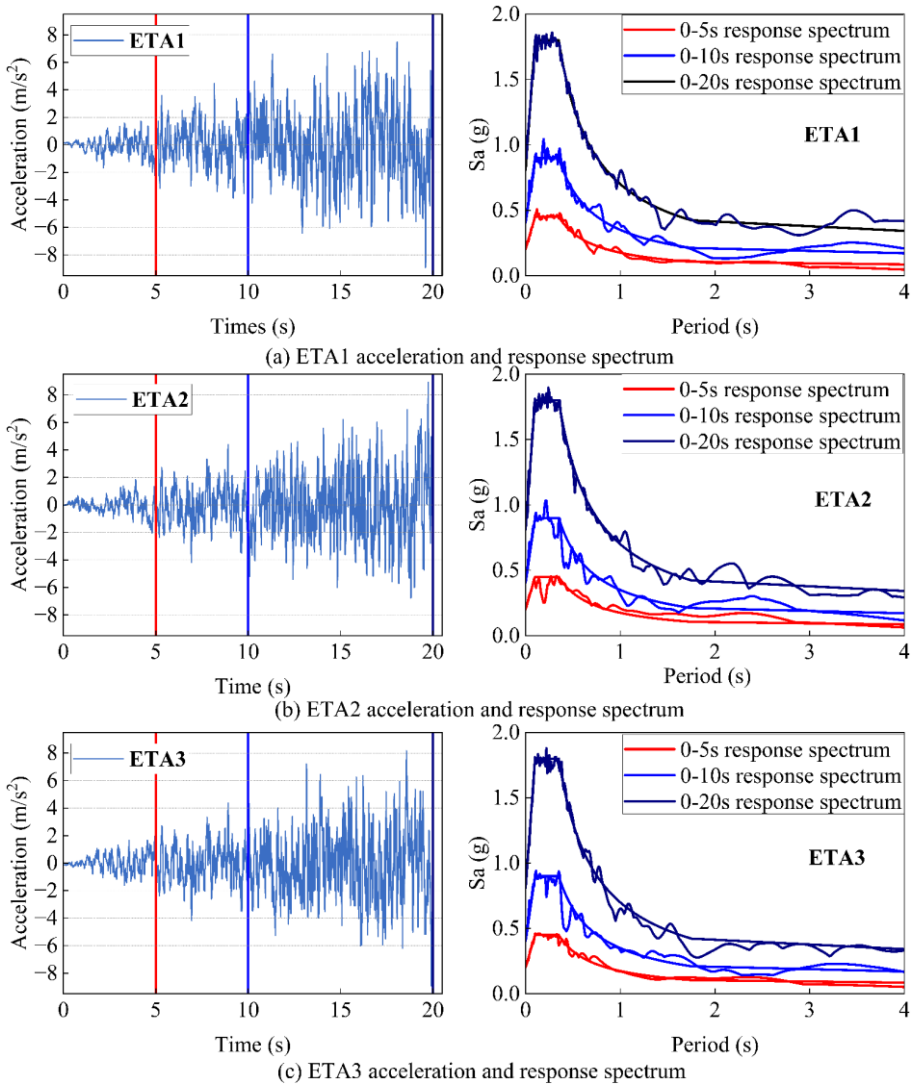

Figure 4 *Three ETACs and response spectrum*

Figure 4 demonstrates that, with time, the peak acceleration of each curve consistently rises, signifying a progressive intensification of the earthquake. Moreover, the comparative examination of response spectra revealed that throughout the aforementioned three periods, the acceleration spectrum of ETACs and the target spectrum exhibited strong fitting characteristics. Consequently, it may be inferred that the three complete ETACs are appropriate for the seismic performance assessment of storage tanks.

4 Collection of seismic response data for storage tanks

4.1 Finite Element Model (FEM) of the storage tank

This research develops a comprehensive finite element model utilizing ADINA software to examine the seismic response of the liquid storage structure. The substantial disparity in thickness between the tank wall and the tank bottom relative to the tank diameter allows it to be classified as a thin-walled structure. In the simulation of thin-walled structures, shell components offer advantages over solid elements for computational efficiency. Potential-based fluid elements have properties like not being able to be seen, not rotating, not conducting electricity, and not being easily compressed. These properties allow the fluid boundary to move slightly. This machine automatically establishes the coupling interface for

fluid-structure interaction analysis, eliminating the requirement for manual configuration. Consequently, the liquid component is represented and analyzed utilizing potential flow units.

Model parameters of the liquid storage tank: volume 2,000 m^3, diameter D=14.5 m, tank height H=12.69 m, thickness of the tank wall and bottom plate t=7 mm, modulus of elasticity of the steel wall and bottom plate E=2.1e11 Pa, Poisson's ratio of the steel υ=0.3, yield limit σ_s=235 MPa, strength limit σ_b=375 MPa, density ρ_s=7850 kg/m^3, storage fluid density ρ_f=1000 kg/m^3, liquid storage volume modulus K=2.1e9 Pa, liquid storage height H_f=11.49 m. The refined finite element numerical simulation model of the tank established in ADINA software is shown in Figure 5.

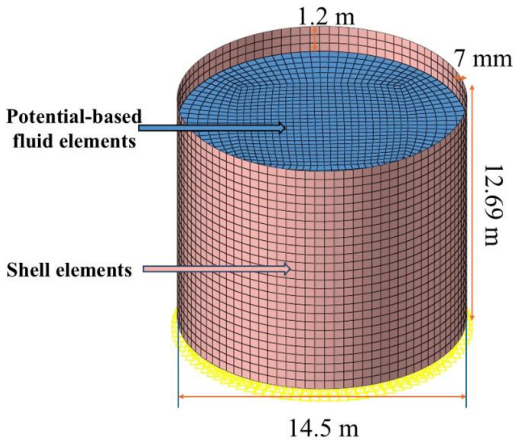

Figure 5 *FEM of the Anchored Storage Tank*

This study compares the fluid-solid coupling vibration frequency with the liquid sloshing frequency, based on the calculation results of formulas D.3.5 and D.3.6 in GB 50341-2014.This standard cites the simplified Haroun-Houner theory model for storage tank analysis; however, the finite element technique considers the storage tank as a thin-walled shell structure, employing shell vibration theory, which aligns more closely with real-world conditions. This research concurrently validates the seismic response of the tank under seismic excitation, assessing the efficacy of base shear, base moment, and wave height. A 2,000 m^3 tank located in the 9-degree zone of a Class III site was chosen for this purpose, and the seismic response under the El Centro 1940 NS earthquake wave (peak acceleration of 0.4 g, duration of 10 s) was compared and validated against the calculation results of formulas D.3.7, D.3.8, and D.3.9 in the standards.

The results in Table 4 indicate that the vibration frequency due to fluid-structure interaction and the fluid sloshing frequency of the storage tank, as computed using the finite element approach, are somewhat lower, though the difference is not substantial. The inaccuracy in the slashing frequency is 1.6%, but the error in the fluid-structure interaction frequency is 3.056%. Furthermore, the discrepancies between the finite element simulation results and the standard calculation values for the base shear force, base moment, and sloshing wave height are 4.9180%, 3.9683%, and 3.2836%, respectively. These findings indicate that the finite element model used in this work is both reliable and accurate.

Table 4 Comparison Analysis of Simulation Numerical Solutions and Standard Solutions

Tank Dynamic Response	Standardized value	Finite element solution	Errors
Frequency of liquid shaking (Hz)	0.250	0.246	1.6000%
Frequency of fluid-solid coupling (Hz)	6.250	6.059	3.0560%
Base shear (kN)	1.22×10^4	1.16×10^4	4.9180%
Base moment (kN·m)	6.30×10^4	6.05×10^4	3.9683%
Sway wave height (m)	0.335	0.324	3.2836%

4.2 Dynamic response analysis and comparison of the storage tank

The h_v、σ_c and σ_v of the storage tank substantially influence the standard operational capacity of the storage structure post-earthquake. Consequently, to thoroughly evaluate the extent of storage damage and its operational efficacy post-earthquake, this study identifies the aforementioned three reaction metrics of the storage tank to represent its seismic response (H.T, 2010). Following the execution of nonlinear ETA on the storage tank, to enable a comparison study of the calculation results from IDA and ETA, the intensity of natural ground motion needs to be converted into the time corresponding to ETA. The equivalent endurance time conversion relationship of ground motion can be expressed by Eq. 11 and Eq.12:

$$\frac{t_{ET}}{\lambda \times S_{aS}(T)} = \frac{t_{Target}}{S_{aC}(T)} \tag{11}$$

$$t_{ET} = \lambda \times \frac{S_{aS}(T)}{S_{aC}(T)} \times t_{Target} \tag{12}$$

In the formula: t_{ET} is the equivalent seismic duration of a single seismic event with different intensities, λ is the amplitude modulation factor of a single seismic event, and S_{aS}(T) is the response spectrum value of a single seismic event record.

The results in Figure 6(a)~(c) indicate that, due to the selection of the greatest dynamic response from the beginning instant to the present, the numerical curves exhibit a progressively rising tendency over time. The ETA calculation results closely align with the IDA results, as the values of the three ETA curves are clustered around the meaning of the IDA results, demonstrating strong concordance. To ensure the continuity and smoothness of the obtained endurance time curves, nonlinear curve fitting is used to fit the median value curve of the tank's dynamic response. The fitted curve overcomes the disadvantage of the fixed seismic response of the structure at certain moments due to the step-like shape of the median. Figure 7(a)~(c) demonstrate that the ETA calculation results closely align with the IDA results. The values of the three ETA curves are clustered around the meaning of the IDA findings, suggesting a strong correlation. This indicates that ETA can more accurately forecast the maximum h_v, maximum σ_c and maximum σ_v of the tank across varying intensities. This suggests that ETA may employ reduced nonlinear analysis to more accurately forecast the maximum dynamic response of the tank, which offers significant benefits and attractiveness for the nonlinear analysis of tanks requiring solid-liquid coupling considerations.

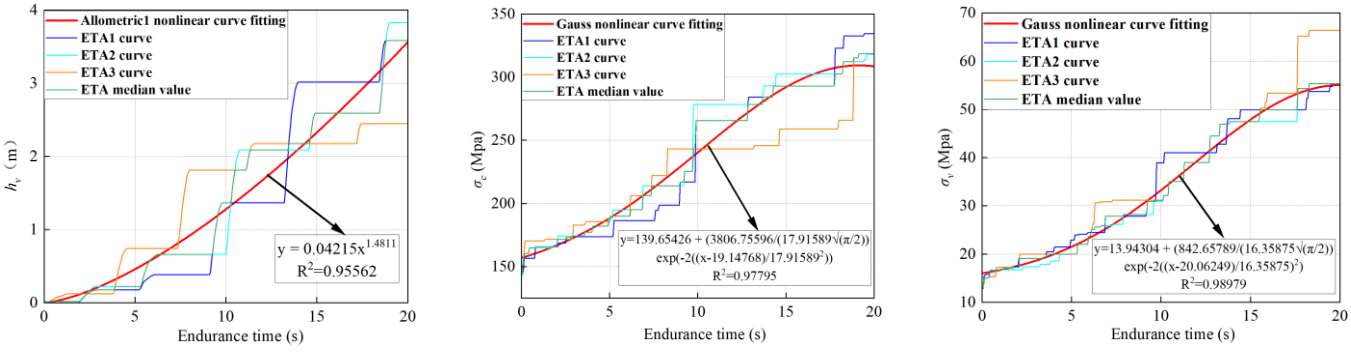

(a) ETA curves of h_v (b) ETA curves of σ_c (c) ETA curves of σ_v

Figure 6 *ETA curves and median nonlinear fitting curves of three seismic performance indicators*

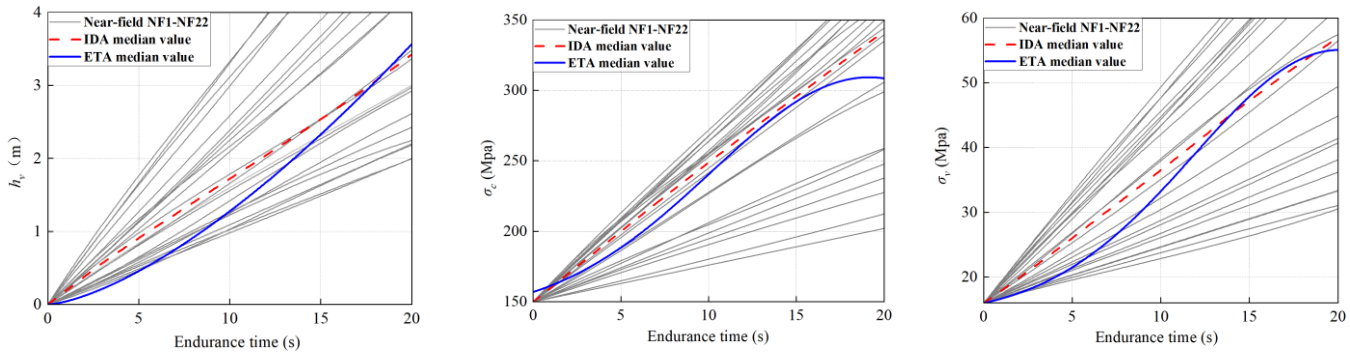

(a) Comparison of h_v (b) Comparison of σ_c (c) Comparison of σ_v

Figure 7 *Results of comparative analysis between ETA and IDA*

After verifying the validity of ETA, seismic parameters can be converted based on the duration. By using a Eq.13 to convert the endurance time into PGA, the seismic response of the storage tank under different PGAs can be obtained. The dynamic response related to PGA will be combined with the dynamic response obtained through Sa to form vector seismic parameters. These will be used to separately conduct vulnerability analysis of the scalar seismic parameters and vector seismic parameters of the storage tank.

$$PGA = \beta \times \frac{t_{ET} \times PGA_C}{t_{Target}} \tag{13}$$

In the equation, t_{ET} is the equivalent seismic duration for different intensities of seismic motion; t_{Target} is the target duration; β is the seismic motion scaling parameter, and PGA_C is the maximum value of the seismic acceleration time history used in IDA.

5 Vulnerability analysis of scalar and vector values of liquid storage tanks

5.1 Scalar value vulnerability analysis results

The preceding section presented curves of vulnerability derived from seismic response, associated with three failure types and five distinct damage states. Vulnerability curves for five damage states—intact, slightly damaged, moderately damaged, severely damaged, and destroyed—were developed in accordance with pertinent formulae. PGA was used as the IM for seismic motion in the assessment of the seismic susceptibility of storage tanks. The vulnerability curves provide a precise assessment of the danger posed to storage tanks during an earthquake. For example, as shown in the Figure 8, when the earthquake PGA is 0.2 g, the likelihood of the storage tank sustaining moderate or greater damage due to the liquid overflow failure mode is below 1%; conversely, when the PGA escalates to 0.8 g, the probability of the storage tank incurring severe damage from the liquid overflow failure mode surpasses 90%, and the probability of total failure also attains 80.56%.The findings suggest that in the failure mode characterized by liquid overflow, when the earthquake PGA is below 0.2 g, the storage tank often remains undamaged; nevertheless, under intense earthquake circumstances, it is more susceptible to significant damage.

The results of the seismic vulnerability analysis of the storage tank using Sa as the IM are illustrated in the figure (8). Figure 9 indicates that while the failure mode analysis employing PGA as the IM demonstrates that the storage tank maintains considerable integrity under weak seismic inputs, it is susceptible to significant damage under intense seismic conditions. Conversely, when Sa is utilized as the IM, the vulnerability analysis of the storage tank exhibits a similar trend. A comparison of the vulnerability curves derived from these two IMs reveals notable discrepancies. For instance, when PGA is 1 g and Sa is 1.8 g, the vulnerability function values constructed based on PGA and Sa differ. In the case of wall

instability as the failure mode, the vulnerability function values derived from PGA are 99.06%, 97.14%, 93.78%, 87.95%, and 76.61%, whereas those derived from Sa are 99.81%, 99.03%, 97.01%, 92.31%, and 80.75%. These data indicate that, although the trends in damage states remain consistent across different IMs, there are discernible differences in the specific probabilities of damage.

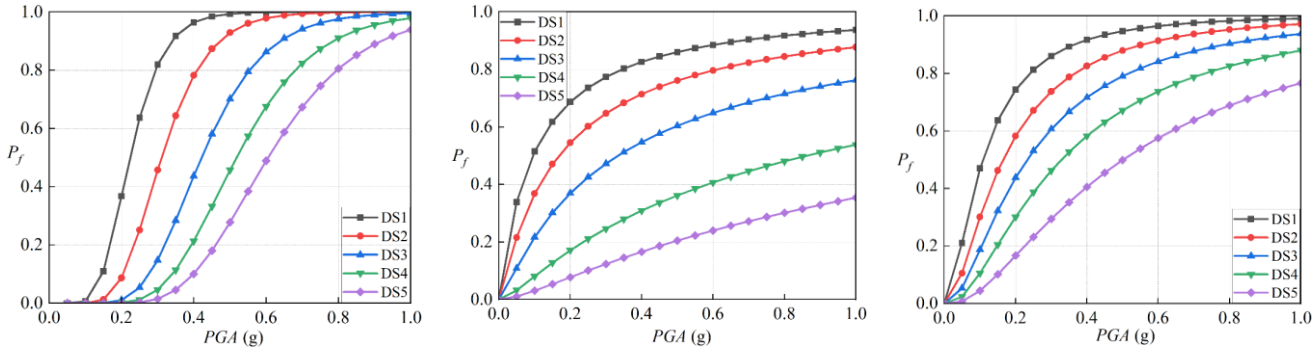

(a) Vulnerability curve of h_v (b) Vulnerability curve of σ_c (c) Vulnerability curve of σ_v

Figure 8 *Vulnerability curve of liquid storage tank using PGA as IM*

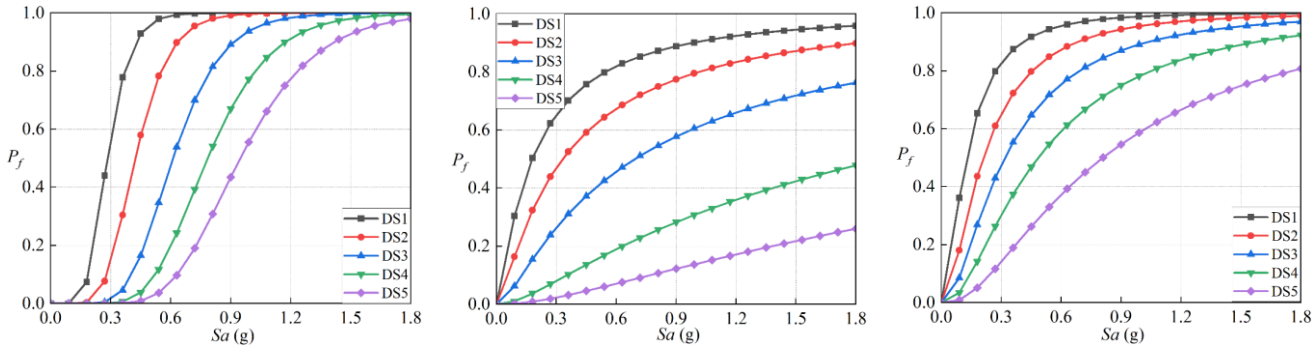

(a) Vulnerability curve of h_v (b) Vulnerability curve of σ_c (c) Vulnerability curve of σ_v

Figure 9 *Vulnerability curve of liquid storage tank with Sa as IM*

5.2 Vector-valued vulnerability analysis results

The analysis in the preceding section indicates that employing a singular scalar IM to develop seismic vulnerability functions may result in substantial variations in damage probabilities, contingent upon the choice of different IMs, consequently influencing the vulnerability assessment outcomes for storage tanks. Conversely, vector intensity measures comprising two ground motion parameters can yield more comprehensive ground motion information for generating probabilistic seismic demand models and seismic vulnerability functions than scalar intensity measures. The utilization of vector IMs surpasses that of scalar IM in several dimensions due to its capacity to provide greater. Therefore, the use of vector IMs can effectively reduce the uncertainty and bias caused by ignoring certain ground motion characteristics, thereby optimizing the results of seismic vulnerability analysis.

In this section, Sa and PGA are used as independent variables, and the maximum h_v, maximum σ_c and maximum σ_v of the liquid storage tank are used as dependent variables to construct a two-parameter logarithmic regression fit as shown in Eq.14 to Eq.16.

$$\ln(h_v) = 1.47\ln(Sa) + 2.145\ln(PGA) - 6.11 \tag{14}$$

$$\ln(\sigma_c) = 0.4616\ln(Sa) + 0.3448\ln(PGA) + 4.0838 \tag{15}$$

$$\ln(\sigma_v) = 0.3853\ln(Sa) + 0.5162\ln(PGA) + 2.1826 \quad (16)$$

By substituting the above regression coefficient value into the vulnerability function proposed in Eq.7, this section can calculate the seismic vulnerability surfaces of 3 different forms and 5 damage states (based on maximum h_v, maximum σ_c and maximum σ_v respectively). These vulnerability surfaces can predict the probability of damage of the storage tank as a function of two IMs, which represent the ground motion. In contrast, the vulnerability probability in the scalar vulnerability analysis method is calculated based on a single IM parameter. As shown in Figure 10 Figure 11 and Figure 12 these vulnerability surfaces can predict the probability of damage of the storage tank, where P_f represents the vulnerability probability. It is not difficult to see that under different damage states, the failure probability of the vulnerability surfaces of maximum h_v, maximum σ_c and maximum σ_v presents a trend of P_f (DS1)> P_f (DS2)> P_f (DS3)> P_f (DS4)> P_f (DS5). The three types of vulnerability transformation trends are basically the same. With the increase of Sa or the increase of PGA, the vulnerability probability will increase. In this section, two ground motion intensity parameters are used as variables. Combined with different damage states, the resulting vulnerability surfaces comprehensively characterize the probability and multi-level of earthquake vulnerability results compared to the vulnerability curves.

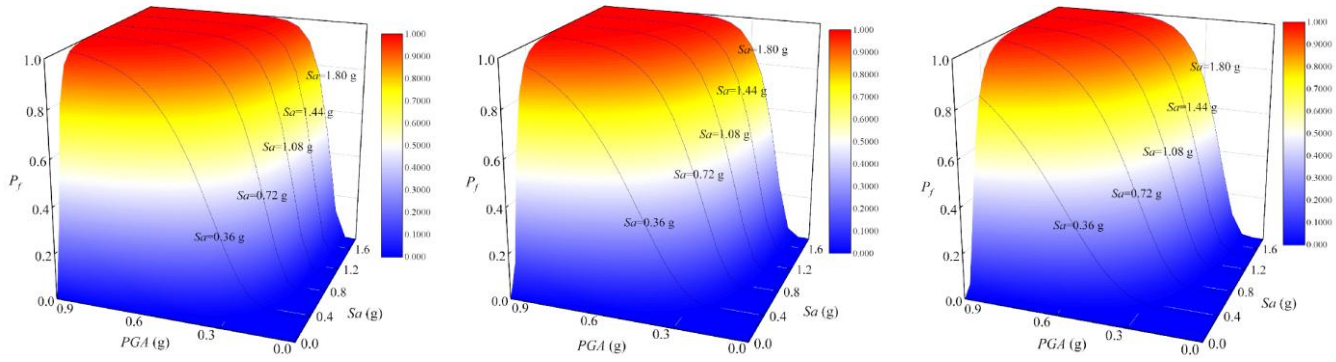

(a) DS1 (b) DS2 (c) DS3

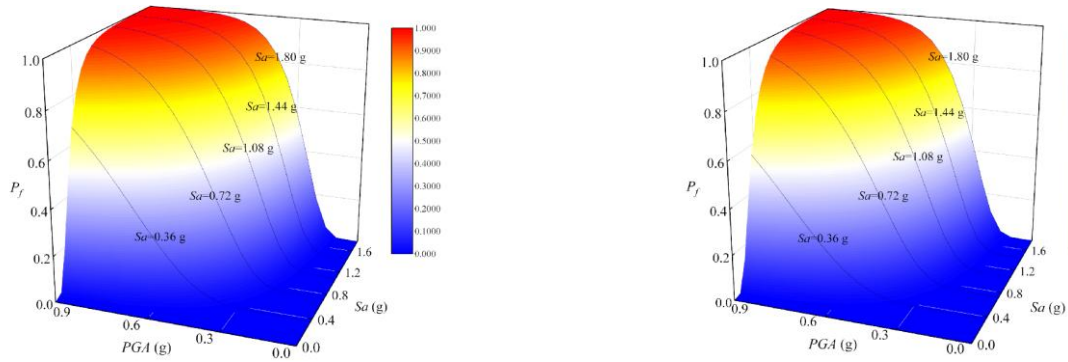

(d) DS4 (e) DS5

Figure 10 *Vulnerability surfaces of h_v under different damage states*

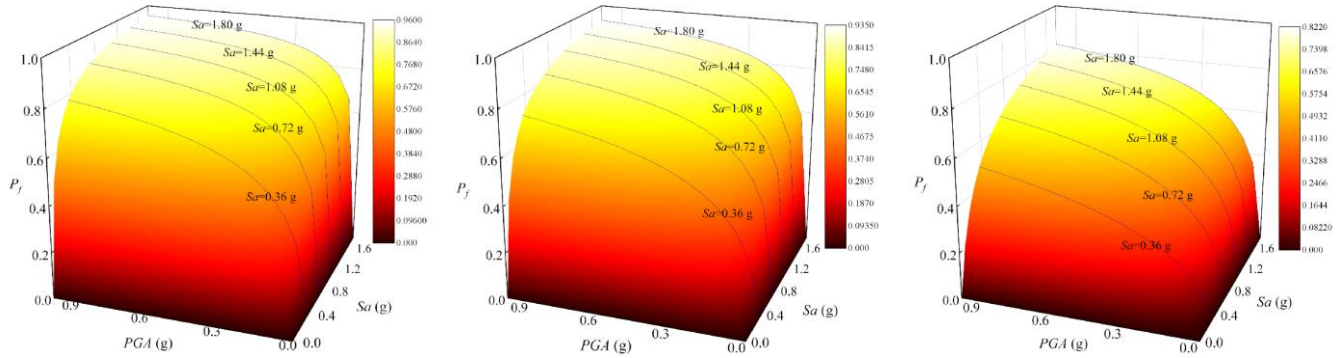

(a) DS1 (b) DS2 (c) DS3

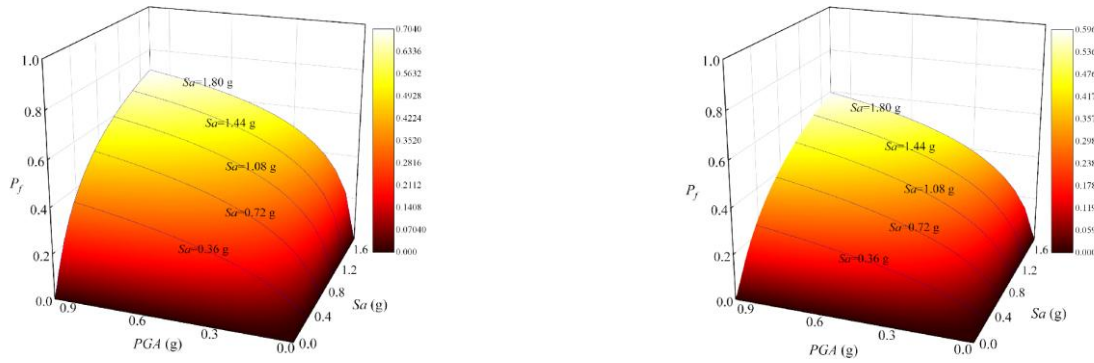

(d) DS4 (e) DS5

Figure 11 *Vulnerability surfaces of σ_c under different damage states*

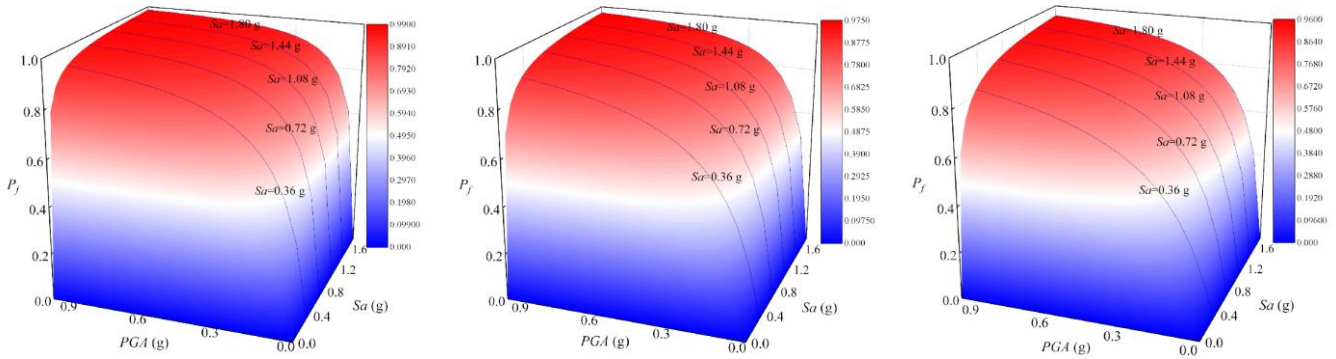

(a) DS1 (b) DS2 (c) DS3

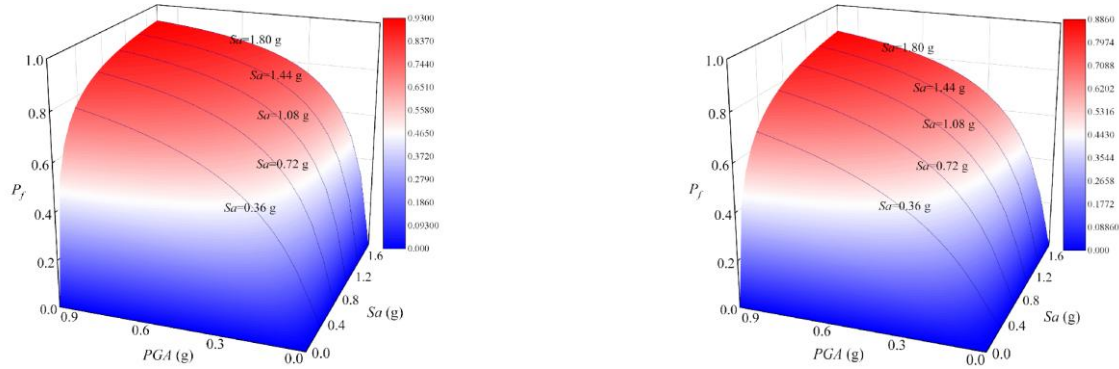

(d) DS4 (e) DS5

Figure 12 *Vulnerability surfaces of σ_v under different damage states*

5.3 Comparison of scalar and vector-valued vulnerability results for storage tanks

Most importantly, the 3D vector vulnerability surface can provide a more accurate representation of vulnerability results than when only one seismic parameter is considered in a probabilistic analysis. The main advantage of the vector-valued vulnerability surface over the scalar-valued vulnerability curve is that it incorporates the effect of the second IM parameter in the vulnerability analysis. To explore the effect of the second IM on the seismic vulnerability of the storage tank, a vulnerability curve based on a single IM can be plotted by keeping one IM constant in the illustrated vector-valued vulnerability surface. To more clearly compare the effects of scalar value IMs and vector value IMs on the tank damage probability, this section fixes the Sa value to five different constants (0.36 g, 0.72 g, 1.08 g, 1.44 g and 1.80 g respectively), and converts the 3D vector value vulnerability surface into a 2D vulnerability curve for direct comparison with the scalar value vulnerability curve. As shown in Figures 13 to 17, there is a significant difference between the vector-valued vulnerability curve and the scalar-valued vulnerability curve, which shows that the damage probability of the liquid storage tank is significantly affected when the second IM constant is maintained. Using a 2D vulnerability curve may underestimate or overestimate the damage risk of the tank.

For example, in the scalar value and vector value vulnerability comparison curve in Figure 15 (b) (under medium damage state), when the input PGA=0.6 g, the constant Sa is 0.36 g, 0.72 g, 1.08 g, 1.44 g, and 1.80 g, the failure probability of the liquid storage tank due to circumferential tensile damage is 26.94%, 41.50%, 50.77%, 57.35%, and 62.32%; the corresponding failure probability of the liquid storage tank in the scalar value brittleness curve is 40.70%; it can be seen that the scalar vulnerability curve relatively underestimates the probability of medium damage to the tank due to circumferential tensile damage of the tank wall. In addition, when the input PGA = 0.8g, in the vector value brittleness curve, the failure probability of constant Sa is 45.83%, 61.61%, 70.17%, 75.65% and 79.5%, respectively, and the corresponding scalar value vulnerability curve has a failure probability of 71.54% for the liquid storage tank. The scalar value vulnerability curve relatively overestimates the probability of medium damage to the tank due to the circumferential tensile strength of the tank wall. Tables 5 and 6 show the failure probabilities of the scalar value and vector value vulnerability curves of the liquid storage tank in different failure modes and different damage states when PGA is 0.6g and 0.8g, respectively.

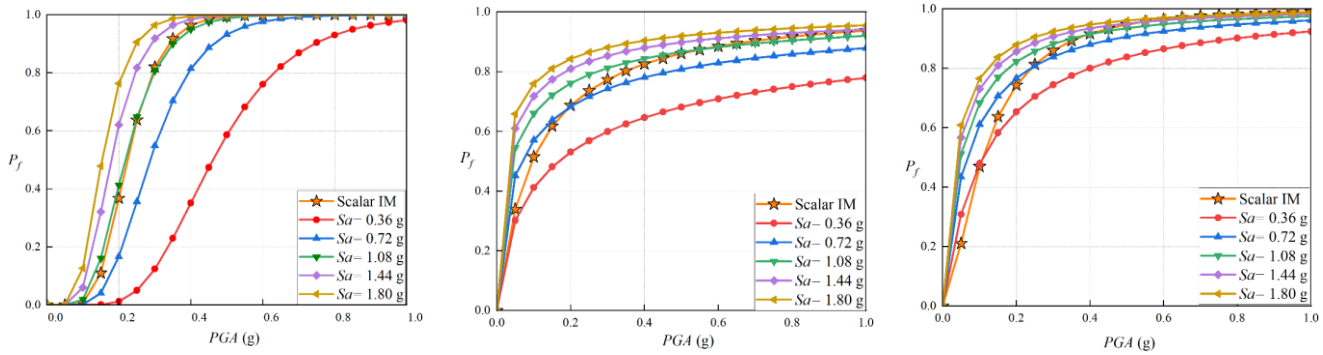

(a) Comparison of damage probability between scalar and vector values of h_v

(b) Comparison of damage probability between scalar and vector values of σ_c

(c) Comparison of damage probability between scalar and vector values of σ_v

Figure 13 *Comparison of vector-valued vulnerability surfaces and scalar-valued vulnerability curves for three failure modes under DS1*

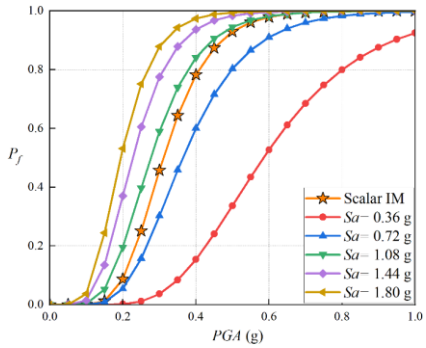

(a) Comparison of damage probability between scalar and vector values of h_v

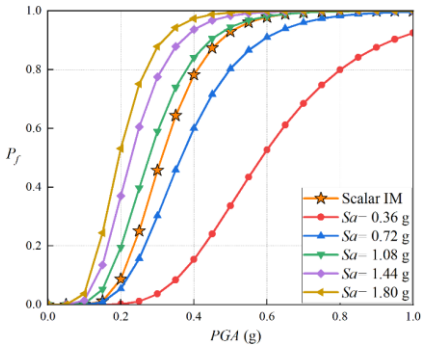

(b) Comparison of damage probability between scalar and vector values of σ_c

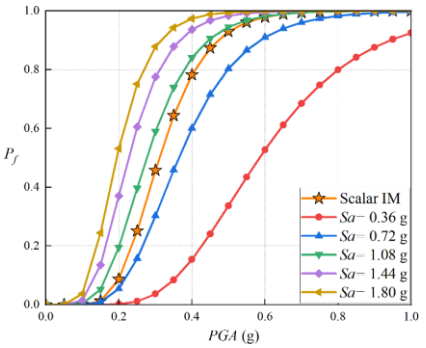

(c) Comparison of damage probability between scalar and vector values of σ_v

Figure 14 *Comparison of vector-valued vulnerability surfaces and scalar-valued vulnerability curves for three failure modes under DS2*

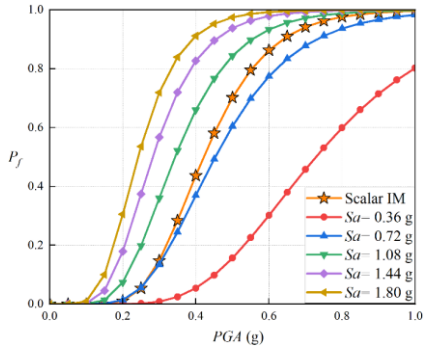

(a) Comparison of damage probability between scalar and vector values of h_v

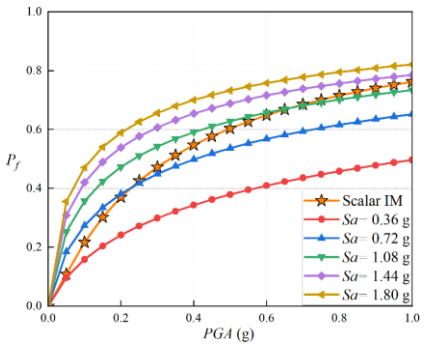

(b) Comparison of damage probability between scalar and vector values of σ_c

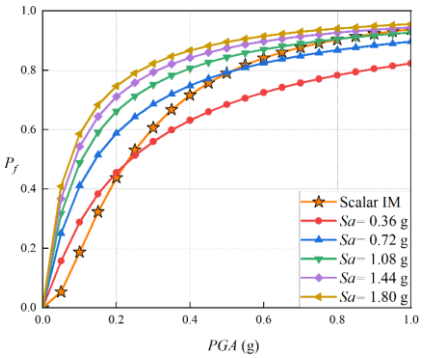

(c) Comparison of damage probability between scalar and vector values of σ_v

Figure 15 *Comparison of vector-valued vulnerability surfaces and scalar-valued vulnerability curves for three failure modes under DS3*

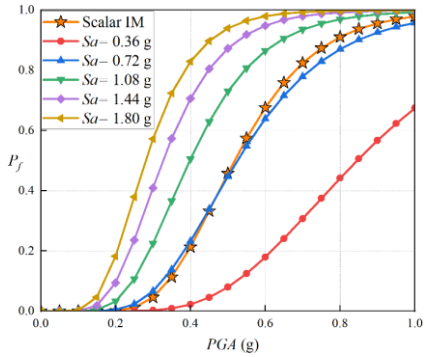

(a) Comparison of damage probability between scalar and vector values of h_v

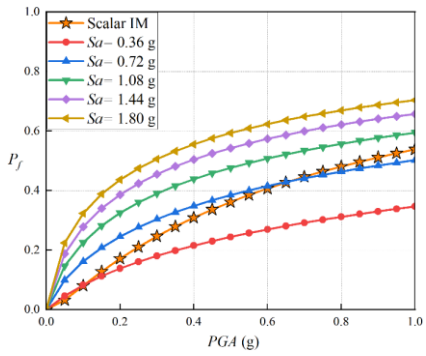

(b) Comparison of damage probability between scalar and vector values of σ_c

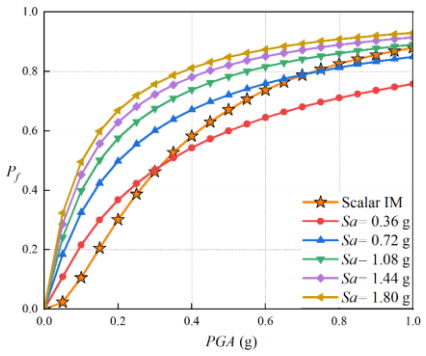

(c) Comparison of damage probability between scalar and vector values of σ_v

Figure 16 *Comparison of vector-valued vulnerability surfaces and scalar-valued vulnerability curves for three failure modes under DS4*

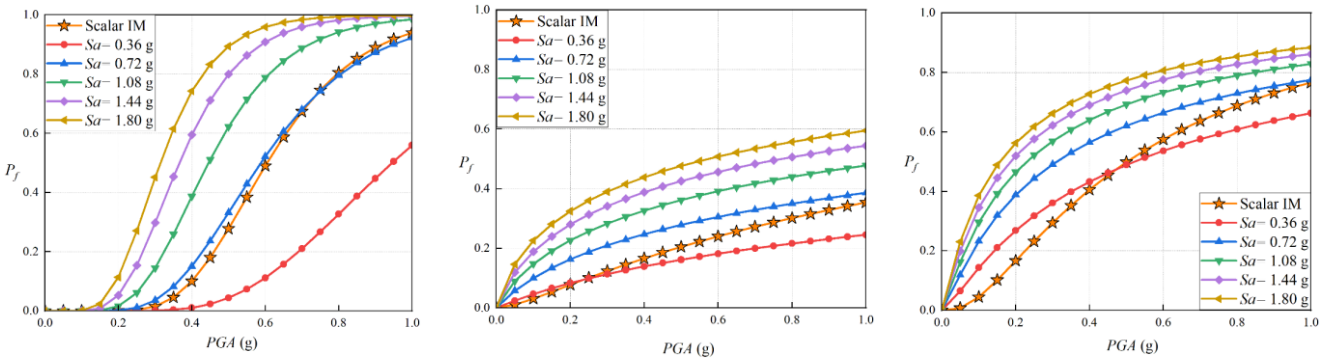

(a) Comparison of damage probability between scalar and vector values of h_v

(b) Comparison of damage probability between scalar and vector values of σ_c

(c) Comparison of damage probability between scalar and vector values of σ_v

Figure 17 *Comparison of vector-valued vulnerability surfaces and scalar-valued vulnerability curves for three failure modes under DS5*

All these results confirm that the vector-valued vulnerability function provides more information than the scalar-valued vulnerability function to characterize the seismic performance of fluid storage tanks. The transformation of the vector-valued vulnerability surface to the vector-valued vulnerability curve can also be presented in the form of common vulnerability curves, which can be applied to the probabilistic seismic risk analysis of fluid storage tanks.

Table 5 Failure probability of vulnerability analysis of scalar and vector ground motion parameters when PGA is 0.6 g.

PGA=0.6 g	Damage Status	Failure probability					
		Scalar IM	Sa=0.36g	Sa=0.72g	Sa=1.08g	Sa=1.44g	Sa=1.80g
h_v	DS1	99.89%	76.00%	97.61%	99.68%	99.94%	99.99%
	DS2	97.90%	52.70%	91.01%	98.15%	99.55%	99.88%
	DS3	86.28%	30.16%	77.45%	93.30%	97.87%	99.26%
	DS4	67.58%	17.93%	63.90%	86.45%	94.84%	97.93%
	DS5	48.95%	11.13%	52.16%	78.79%	90.79%	95.89%
σ_c	DS1	88.52%	70.90%	82.90%	88.19%	91.15%	93.04%
	DS2	79.63%	63.65%	77.31%	83.72%	87.47%	89.94%
	DS3	64.88%	40.95%	56.80%	65.73%	71.60%	75.80%
	DS4	40.70%	26.94%	41.50%	50.77%	57.35%	62.32%
	DS5	23.99%	18.16%	30.53%	39.16%	45.65%	50.78%
σ_v	DS1	96.49%	86.53%	92.48%	94.88%	96.18%	96.99%
	DS2	91.37%	79.55%	87.69%	91.22%	93.23%	94.53%
	DS3	84.12%	72.50%	82.42%	87.01%	89.71%	91.51%
	DS4	73.72%	64.42%	75.91%	81.56%	85.02%	87.39%
	DS5	57.47%	53.62%	66.44%	73.23%	77.59%	80.67%

Table 6 Failure probability of vulnerability analysis of scalar and vector ground motion parameters when PGA is 0.8 g.

PGA=0.8 g	Damage Status	Failure probability					
		Scalar IM	Sa=0.36g	Sa=0.72g	Sa=1.08g	Sa=1.44g	Sa=1.80g
h_v	DS1	99.99%	93.02%	99.7%	99.98%	100%	100%
	DS2	99.83%	79.93%	98.27%	99.79%	99.97%	99.99%
	DS3	97.62%	59.93%	93.64%	98.84%	99.74%	99.93%
	DS4	91.06%	44.17%	87.01%	96.94%	99.18%	99.75%
	DS5	80.56%	32.71%	79.55%	94.19%	98.21%	99.4%
σ_c	DS1	91.75%	75%	85.87%	90.46%	92.98%	94.55%
	DS2	84.51%	68.2%	80.87%	86.59%	89.85%	91.95%
	DS3	71.54%	45.83%	61.61%	70.17%	75.65%	79.5%
	DS4	48.07%	31.18%	46.39%	55.69%	62.14%	66.93%
	DS5	30.17%	21.62%	35.01%	43.99%	50.59%	55.71%
σ_v	DS1	98.27%	90.15%	94.78%	96.56%	97.49%	98.06%
	DS2	95.22%	84.4%	91.07%	93.83%	95.34%	96.3%
	DS3	90.36%	78.33%	86.8%	90.53%	92.66%	94.04%
	DS4	82.57%	71.07%	81.31%	86.09%	88.93%	90.83%
	DS5	68.83%	60.89%	72.92%	78.97%	82.74%	85.35%

6 Conclusion

This paper introduces ETA to study the vulnerability analysis of liquid storage tanks, which is used to evaluate the seismic performance of liquid storage tanks. The finite element model of the liquid storage tank is constructed, and then the seismic dynamic response of the liquid storage tank is obtained by selecting different seismic waves for incremental dynamic analysis and generating 3 endurance time acceleration curves for ETA analysis. Then different scalar value vulnerability curves are constructed. Considering that a single IM may not reliably characterize the seismic record, the dynamic response of PGA is obtained through seismic time history analysis conversion, and the vector value vulnerability surface of PGA and Sa is constructed to further evaluate the seismic vulnerability of the liquid storage tank. The main conclusions are as follows:

(1) ETA can fully reflect the process of the liquid storage tank from being intact to gradually damaged and finally failing. Through a single endurance time calculation, the ultimate seismic resistance of the liquid storage structure can be roughly determined, which can greatly reduce the calculation workload of seismic analysis.

(2) The scalar vulnerability curves of PGA and Sa were constructed. The results showed that the vulnerability curves constructed by two different ground motion parameters showed roughly the same trend when evaluating the vulnerability analysis of the liquid storage tank, but there were still differences depending on the selected IM.

(3) Considering that a single IM may not be sufficient to fully and effectively characterize earthquake records, a vector-valued vulnerability surfaces represented by PGA and Sa is also constructed for seismic vulnerability analysis of liquid storage tanks with different damage states. The introduction of a second IM in seismic vulnerability analysis and the development of a vector-valued vulnerability surface can more accurately assess the seismic hazard of liquid storage tanks.

Acknowledgments

The work described in this paper was fully supported by the National Natural Science Foundation of China (Grant No. 50978064) and the Science and Technology Foundation of Guizhou Province (Project No. 20092010). Their support is sincerely appreciated.

Author's Contribuitions: Conceptualization, Yi Yang; Methodology, Yi Yang and Jianchun Xiao; Investigation, Cong Liu; Writing - original draft, Yi Yang; Writing - review & editing, Yi Yang; Funding acquisition, Jianchun Xiao; Resources, Jun Wang.

Editor: Rogério José Marczak

References

(2014) GB 50341-2014 (2014 Edition) Code for design of vertical cylindrical welded steel oil tanks. Beijing: China Planning Press.

(2016) GB 50011-2016 (2016 Edition) Code for Seilsmic Design of Buildings. Beijing: China Construction Industry Press.

(2009) GB/T 24336-2009 (2009 Edition) Classification of earthquake damage levels for lifeline projects. Beijing: China Standards Press.

(2018) GB/T 50761-2018 (2018 Edition) Seismic design standard for petrochemical steel equipment. Beijing: China Planning Press.

Akköse M, Adanur S, Bayraktar A, et al. (2008). Elasto-plastic earthquake response of arch dams including fluid–structure interaction by the Lagrangian approach. Applied Mathematical Modelling 32(11): 2396–2412.

Alessandri S, Caputo AC, Corritore D, et al. (2018). Probabilistic risk analysis of process plants under seismic loading based on Monte Carlo simulations. Journal of Loss Prevention in the Process Industries 53: 136–148.

Argyroudis SA, Pitilakis KD. (2012). Seismic fragility curves of shallow tunnels in alluvial deposits. Soil Dynamics and Earthquake Engineering 35: 1–12.

Baker JW. (2007). Probabilistic structural response assessment using vector-valued intensity measures. Earthquake Engineering & Structural Dynamics 36(13): 1861–1883.

Bektaş N , Aktaş E. (2023). Seismic Vulnerability Assessment of an Unanchored Circular Storage Tank Against Elephant's Foot Buckling. Journal of Vibration Engineering & Technologies 11(4): 1661–1678.

Brunesi E, Nascimbene R, Pagani M, et al. (2015). Seismic Performance of Storage Steel Tanks during the May 2012 Emilia, Italy, Earthquakes. Journal of Performance of Constructed Facilities 29(5): 04014137.

Chen G, Jin D, Mao J, et al. (2014). Seismic damage and behavior analysis of earth dams during the 2008 Wenchuan earthquake, China. Engineering Geology 180: 99–129.

Chiang J, Wong MS. (2014). Seismic Analysis of Reinforced Concrete Structures in Low to Moderate Earthquake Zones of Peninsular Malaysia. In: Hassan R, Yusoff M, Ismail Z, et al. (eds) InCIEC 2013. Singapore: Springer Singapore, pp. 225–236.

Cornell CA, Jalayer F, Hamburger RO, et al. (2002). Probabilistic Basis for 2000 SAC Federal Emergency Management Agency Steel Moment Frame Guidelines. Journal of Structural Engineering 128(4): 526–533.

De Angelis M, Giannini R , Paolacci F. (2010). Experimental investigation on the seismic response of a steel liquid storage tank equipped with floating roof by shaking table tests. Earthquake Engineering & Structural Dynamics 39(4): 377–396.

Erkmen B. (2024). Seismic performance assessment of an existing anchored and a self-anchored liquid storage tank in high seismic regions. Bulletin of Earthquake Engineering 22(8): 4197–4217.

Estekanchi HE, Valamanesh V , Vafai A. (2007). Application of Endurance Time method in linear seismic analysis. Engineering Structures 29(10): 2551–2562.

Estekanchi HE, Vafai A and Sadeghazar. (2004). Endurance Time Method for Seismic Analysis and Design of Structures.

Cui W, Liu G, Zhang S, et al. (2023). Seismic performance evaluation of gravity dam considering oblique incidence using seismic time history

method, Journal of Hydroelectric Engineering 42 (2023) 132–145.

Zhang C, Zhou Z, Lai Z, et al. (2022). Elastic-plastic seismic response and damage development of reinforced concrete frames based on seismic time history method, World Earthquake Engineering 38 (2022) 44–53.

Chen D, Wang R, Lin T, et al. (2024). Seismic vulnerability analysis of high arch dam based on seismic time history method, Journal of Hydroelectric Engineering 43 (2024) 108–119.

Wang G, Wang H, Wang J, et al. (2024). Study on seismic performance of underground structures subjected to sequential earthquakes based on seismic time history method, Journal of Vibration and Shock 43 (2024) 261-268+276.

Huang J, Tan P, Zhang Y, et al. (2024). Application of seismic time history method in longitudinal seismic performance evaluation of long-span continuous rigid frame bridges, Journal of Vibration Engineering 37 (2024) 306–317.

Hajimehrabi H, Behnamfar F, Samani AK, et al. (2019). Fragility curves for baffled concrete cylindrical liquid-storage tanks. Soil Dynamics and Earthquake Engineering 119: 187–195.

He Z, Xu H, Gardoni P, et al. (2022). Seismic demand and capacity models, and fragility estimates for underground structures considering spatially varying soil properties. Tunnelling and Underground Space Technology 119: 104231.

Huang Z-K, Pitilakis K, Argyroudis S, et al. (2021). Selection of optimal intensity measures for fragility assessment of circular tunnels in soft soil deposits. Soil Dynamics and Earthquake Engineering 145: 106724.

H.T. R. (2010). Seismic assessment of steel frames with the endurance time method. Journal of Constructional Steel Research 66(6). Elsevier: 780–792.

Kildashti K, Mirzadeh N, Samali B. (2018). Seismic vulnerability assessment of a case study anchored liquid storage tank by considering fixed and flexible base restraints. Thin-Walled Structures 123: 382–394.

Matsui T. (2009). Sloshing in a Cylindrical Liquid Storage Tank With a Single-Deck Type Floating Roof Under Seismic Excitation. Journal of Pressure Vessel Technology 131(2): 021303.

Melchers R E.(1999). Structural Reliability: Analysis and Prediction[M]. 2nd Edition, JohnWiley, New York, NY.

Merino Vela RJ, Brunesi E, Nascimbene R. (2018). Derivation of floor acceleration spectra for an industrial liquid tank supporting structure with braced frame systems. Engineering Structures 171: 105–122.

Merino Vela RJ, Brunesi E, Nascimbene R. (2019). Seismic assessment of an industrial frame-tank system: development of fragility functions. Bulletin of Earthquake Engineering 17(5): 2569–2602.

Miladi S, Razzaghi MS, Ghasemi SH. (2022). Seismic performance of imperfect unanchored tanks. Proceedings of the Institution of Civil Engineers - Structures and Buildings 175(7): 551–560.

Nozari A, Estekanchi HE. (2011). OPTIMIZATION OF ENDURANCE TIME ACCELERATION FUNCTIONS FOR SEISMIC ASSESSMENT OF STRUCTURES. Iran University of Science & Technology 1(2). Iran University of Science & Technology: 257–277.

Sun B, Deng M, Zhang S, et al. (2021). Application of the endurance time methodology on seismic analysis and performance assessment of hydraulic arched tunnels. Tunnelling and Underground Space Technology 115: 104022.

Sun J, Zhang R, Jiang F, et al. (2009). Numerical simulation analysis of seismic vulnerability of storage tanks, Journal of Harbin Institute of Technology 41 138–142.

Tavakoli Joorabi A, Razzaghi MS. (2019). Seismic fragility analysis of retrofitted steel tanks considering corrosion. Proceedings of the Institution of Civil Engineers - Structures and Buildings 172(10): 712–720.

Valamanesh V, Estekanchi HE, Vafai A. (2010). Characteristics of Second Generation Endurance Time Acceleration Functions.

Vasquez Munoz LE, Dolšek M. (2024). Parametric seismic fragility model for elephant-foot buckling in unanchored steel storage tanks. Bulletin of Earthquake Engineering 22(11): 5775–5804.

Wang X, Chen J, Xiao M. (2018). Seismic damage assessment and mechanism analysis of underground powerhouse of the Ying xiu wan Hydropower Station under the Wenchuan earthquake. Soil Dynamics and Earthquake Engineering 113: 112–123.

Yu X, Li Y, Song P, et al. (2021). Study on the influence of limit state fuzziness on seismic vulnerability analysis: A case study of reinforced concrete frame structure, Engineering Mechanics 38 (2021) 89-99+109.